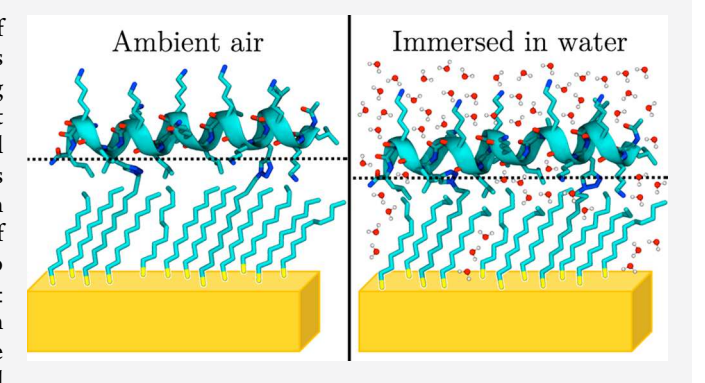
Quantifying the Extent of Hydration of a Surface-Bound Peptide **Using Neutron Reflectometry**

Whitney A. Fies,^{†,∥} Jeremy T. First,^{†,∥} Jason W. Dugger,^{‡,⊥} Mathieu Doucet,[§] James F. Browning,[§] and Lauren J. Webb*, To

Supporting Information

ABSTRACT: Establishing how water, or the absence of water, affects the structure, dynamics, and function of proteins in contact with inorganic surfaces is critical to developing successful protein immobilization strategies. In the present article, the quantity of water hydrating a monolayer of helical peptides covalently attached to self-assembled monolayers (SAMs) of alkyl thiols on Au was measured using neutron reflectometry (NR). The peptide sequence was composed of repeating LLKK units in which the leucines were aligned to face the SAM. When immersed in water, NR measured 2.7 \pm 0.9 water molecules per thiol in the SAM layer and between 75 ± 13 and 111 ± 13 waters around each peptide. The quantity of water in the SAM was nearly twice that measured



prior to peptide functionalization, suggesting that the peptide disrupted the structure of the SAM. To identify the location of water molecules around the peptide, we compared our NR data to previously published molecular dynamics simulations of the same peptide on a hydrophobic SAM in water, revealing that 49 ± 5 of 95 ± 8 total nearby water molecules were directly hydrogen-bound to the peptide. Finally, we show that immersing the peptide in water compressed its structure into the SAM surface. Together, these results demonstrate that there is sufficient water to fully hydrate a surface-bound peptide even at hydrophobic interfaces. Given the critical role that water plays in biomolecular structure and function, these results are expected to be informative for a broad array of applications involving proteins at the bio/abio interface.

■ INTRODUCTION

The specificity, efficiency, and broad-spectrum functionality of proteins make them desirable materials for use in a wide range of applications, including biosensors, biofuel cells, or drug delivery technologies. Capitalizing on proteins for these purposes often requires immobilizing proteins to inorganic surfaces, such as to an electrode for a biosensor or a substrate for heterogeneous catalysis. Beyond a few specific examples, accomplishing this has been difficult because of the structural, and therefore functional, instability of proteins on artificial materials and outside the well-regulated environment of a cell. 1-3 As a result, stabilizing surface-immobilized proteins is an ongoing challenge, with many outstanding questions on the physical and chemical forces that control protein structure and function at abiological surfaces.³⁻⁷ In particular, biomolecular structure is critically dependent on interactions with water in its local solvation environment.^{8–10} Truly generalizable biofunctionalization strategies have been inhibited by a lack of understanding of the role of water in the perturbed chemical, structural, and electrostatic environment at inorganic

surfaces. A significant amount of work has demonstrated that the structure of surface-bound proteins is strongly dependent on the hydrophobicity and charge of the surface to which they are tethered. 11-17 Furthermore, even in cases where the protein structure is not perturbed, surface charges can impact the electrostatic environment of the protein, altering its function. 18,19 However, efforts specifically focused on measuring the role of water in stabilizing a protein that has been intentionally immobilized on an abiological surface are underrepresented; a few studies have measured how the level of hydration of the protein or underlying substrate causes conformational changes and changes in enzyme activity, but the location of specific water molecules and their abundance have not been systematically studied.^{20,21}

Water plays a central role in protein structure and function; it influences a protein by driving the hydrophobic collapse of

Received: August 15, 2019 Revised: November 12, 2019 Published: December 17, 2019

Department of Chemistry and Texas Materials Institute, The University of Texas at Austin, 2506 Speedway STOP A5300, Austin, Texas 78712, United States

[‡]Center for Nanophase Materials Sciences, Oak Ridge National Laboratory, Oak Ridge, Tennessee 37830, United States

[§]Neutron Scattering Division, Oak Ridge National Laboratory, Oak Ridge, Tennessee 37831, United States

the protein core and acts as a proton donor in catalysis, among many other functions. Furthermore, dehydrating a protein can critically disrupt its structure and function by a variety of mechanisms, such as deteriorating hydrogen bonds that stabilize a native tertiary structure. Y-ray crystallography, neutron diffraction, and NMR have historically been used to locate structural waters in and around proteins in crystals or solution. Advances in ultrafast spectroscopy have led to measurements of the dynamics of protein hydration shells which fluctuate on picosecond time scales. Although these techniques continue to elucidate the location and function of water required for protein function, for the most part they are inapplicable to proteins immobilized on inorganic surfaces.

Characterizing water at the protein-surface interface remains challenging because of the relatively few techniques that directly detect water at surfaces and interfaces. Indirectly, multiple analytical techniques have been used to show that hydration plays an essential role in the functionality of immobilized proteins. For instance, electron paramagnetic resonance studies on immobilized enzymes immersed in an organic polar solvent determined that enzyme flexibility increased with an increase in the water content of the solvents.²⁵ Likewise, differential scanning calorimetric studies of proteins absorbed onto mesoporous silicate suggested that the hydrogen bonding nature of silicate increases the hydration level of proteins, which directly contributed to an increase in their thermal stability. 26 Although studies such as these emphasized the importance of hydration on protein dynamics, they lacked the ability to locate water at the interfaces, and therefore they lacked mechanistic evidence that water molecules were responsible for observed changes in stability or function. A more direct method for measuring structural changes of biomolecules in contact with surfaces is vibrational sum frequency generation (SFG) spectroscopy, which has submonolayer sensitivity to detect local environmental changes around C-H, amide, and other protein vibrational modes.² Changes in these vibrational modes can be detected as the amount of water changes in the vicinity of the vibrational transition, providing information on structural fluctuations induced by the presence of water. As a result, SFG has detected the location of water in disordered self-assembled monolayers (SAMs) of siloxanes^{28,29} and has shown that the hydration shell of proteins is disrupted when in contact with poly-(ethylene glycol). 30 However, directly quantifying the extent of solvation in and around a surface-immobilized protein remains elusive.

In contrast to the aforementioned techniques, neutron reflectometry (NR) can directly detect water at an interface between multiple laminae, such as a monolayer of protein between an inorganic surface to which it is immobilized and bulk water. Furthermore, this technique is nondestructive to soft biological materials and can determine the isotopic composition of each lamina. By selectively deuterating the solvent or surface structures through a method known as "contrasting," NR can detect the location and concentration of water in different layers of a system with subnanometer resolution. These advantages make it an ideal tool for locating water surrounding immobilized proteins on abiotic surfaces. Consequently, NR has been successfully used to measure the hydration of antifouling surfaces,³¹ amelogenin peptide adsorbed onto carboxylic acid-terminated SAMs,³² supported lipid bilayers,³³ and bacterial proteins recrystallized on polyelectrolyte multilayers.34

Similarly, molecular dynamics (MD) simulations are able to directly assess the role of water in the stability of proteins at various surfaces. The accuracy of these simulations, however, is entirely dependent on the accuracy of the underlying potential energy function, and therefore the simulations must be validated against experimental data. Once validated, MD simulations are useful at generating molecular structures to assist in the interpretation of experimental data. For example, MD simulations determined that the self-assembly of two synthetic amphiphilic peptides at the air-water interface formed a cooperatively ordered monolayer with only partial helical content, even though each peptide individually forms completely helical monolayers.³⁵ The thickness and density of these monolayers were verified with NR, but MD simulations were able to elucidate the actual peptide structure. The simultaneous use of simulations coupled to experiments in this way advances our molecular-level understanding of protein structure and function.

Previously, we have demonstrated a method for functionalizing short peptides to SAMs on Au. Peptides were covalently bound to mixed SAMs composed of 25% azide-terminated alkyl thiols and 75% methyl-terminated alkyl thiols through a Cu(I)-catalyzed Huisgen cycloaddition (better known as a "click" reaction) between the SAM azides and two alkynes incorporated in the peptide sequence through unnatural amino acids. One peptide we have used in this approach is LKKLXKKLLKKLLKKXLKKL, where X is propargylglycine (hereafter referred to as α LK2x20). This peptide was designed by DeGrado and Lear to adopt an α -helical conformation at hydrophobic-hydrophilic interfaces, placing the hydrophilic lysine residues and hydrophobic leucine residues on opposing sides of the helical axis.³⁶ Indeed, we have shown that this peptide assumes a stable α -helical structure parallel to the Au surface upon binding to a hydrophobic SAM surface.³⁷ These surfaces have been extensively characterized with Fourier transform infrared (FTIR) spectroscopy, X-ray photoelectron spectroscopy (XPS), ellipsometry, circular dichroism (CD) spectroscopy, and scanning tunneling microscopy (STM) to confirm the peptide structure and ensure complete monolayer ⁴⁰ Importantly, however, none of these characterformation.³⁷ ization methods were able to address the extent of hydration of the peptide on the surface when immersed in aqueous solution. More recently, we reported MD simulations that accurately captured conformational changes for this peptide induced by the SAM surface in an aqueous solution; the simulations were in quantitative agreement with structural assignments from CD spectra. 41 Although the combination of experimental techniques and simulations provided a detailed characterization of the peptide structure on the SAM surface, we now aim to quantify the extent of peptide hydration, to measure how much water is associated with the peptide, and to determine where the water is located. This is an extension of recent work using NR in which we reported the direct measurement of water penetrating an alkyl thiol SAM, which is usually assumed to be impervious to water because of its hydrophobicity. 42 Building on these previous results, the new NR experiments discussed here further explore the quantity and location of water at the bio/abio interface.

In this report, we used NR to quantify water located in the vicinity of α LK2x20 while covalently bound to a hydrophobic alkyl thiol SAM on Au. These results are compared with MD simulations of α LK2x20 on SAMs and in water. Comparing the height and area of the peptide in MD simulations to the NR

data allowed us to interpret the structure of α LK2x20 tethered to the SAM surface in air versus immersion in water. MD simulations also provided molecular information on the location of the water molecules associated with the peptide that were experimentally observed by NR. Reflectivity data of peptide-functionalized surfaces were obtained in ambient air and in contrasting aqueous environments, which were achieved by immersing the surface in D₂O and a 70/30 v/v mixture of D₂O/H₂O. NR analysis revealed that αLK2x20 was densely packed on the surface and that the peptide interacted with the SAM layer in a manner that induced disorder in the SAM. When the surface was immersed in water, both the SAM and the peptide layer interacted with water molecules. Our NR results are in good agreement with the quantity of water calculated within the same molecular volume of aLK2x20 using MD simulations, which revealed that each peptide was accompanied by at least a full solvation shell of water. Furthermore, MD simulations resolved that approximately half of these water molecules were hydrogen bound to the peptide. This information will be vital for understanding the structure, dynamics, and function of immobilized peptides in hydrated environments. Because water plays an essential role in protein stability, the results presented here contribute to developing successful immobilization strategies for many biotechnological applications.

■ EXPERIMENTAL SECTION

Surface Functionalization. Neutron reflectometry experiments required the use of single-crystal, round Si(111) 50.8-mm-diameter and 5-mm-thick wafers (University Wafer or El-Cat) that were kept in the original packing in a glovebox under an inert atmosphere before use. Wafers were used as received. Metal deposition was carried out in a class 100/1000 cleanroom with a Cooke electron beam evaporator under a vacuum of $\leq 10^{-6}$ Torr. Samples used in this work were from two different deposition batches. In one batch, approximately 1 nm of Cr (Kurt Lesker) and then 20 nm of Au (Kurt Lesker, 99.95% purity) were deposited on the polished side of the wafers while the substrates were maintained at $110\,^{\circ}$ C. In the second batch, deposition was completed in the same manner but with 5 nm of Cr and 40 nm of Au. Formation of the SAM began within 1 h of Au deposition.

Peptide functionalization of Au was completed in three steps. First, SAMs were formed by incubating the Au substrate in a solution of 0.25 mM 11-bromo-1-undecanethiol (Sigma-Aldrich) and 0.75 mM deuterated d_{21} -decanethiol (C/D/N Isotopes) dissolved in ethanol for at least 24 h at room temperature in the dark. Each sample was rinsed by immersing it in solvent with convection for ≥ 1 min in high-purity water (HPW) from a Barnstead Nanopure purification system (18.2 $M\Omega$ cm) and then ethanol. Samples were dried under a stream of $N_2(g)$. In the second step, SAMs were transferred into a saturated solution of NaN3 in N,N-dimethylformamide (DMF) and incubated at room temperature in the dark for 36 to 48 h to replace the Br with N₃. 40,43 The samples were then rinsed consecutively in solvents DMF, HPW, DMF, HPW, and ethanol before drying under a stream of $N_2(g)$. The final mixed SAM was composed of 25% azide- and 75% methyl-terminated thiols, referenced throughout this work as 25AzUDT. In the third and final step, a peptide was covalently attached to the SAM by a Cu(I)-catalyzed Huisgen cycloaddition (or click reaction) between the N₃ groups of the SAM and alkyne groups on the peptide. The peptide used here, αLK2x20 (Wuxi Corporation, MW 2395.2), had the sequence LKKLXKKLLKKLLKKXLKKL-COOH in which X was the artificial amino acid propargylglycine. The cycloaddition was accomplished by immersing the SAM in 2:1 v/v tbutanol/water containing 10 µM peptide, 20 µM CuSO₄ (Ricca Chemical), 140 µM sodium ascorbate (Sigma-Aldrich), and 20 µM Tris[(1-benzyl-1H-1,2,3-triazol-4-yl)methyl]amine (TBTA, Sigma-Aldrich) with a total volume of 50 mL. The reactants were added to the solvent in the following order: peptide, TBTA, sodium

ascorbate, SAM, and CuSO₄. Each vessel was sealed with electrical tape and incubated at 70 \pm 3 $^{\circ}$ C in the dark for 6 h. Reacted samples were allowed to cool to room temperature prior to cleaning. Samples were rinsed with convection for ≥ 1 min in 2:1 *t*-butanol/water, HPW, 1× phosphate-buffered saline, HPW again, and ethanol and then dried under a stream of N₂(g). All peptide-functionalized surfaces were stored in wafer cassettes in the dark at room temperature until further analysis. A depiction of $\alpha LK2x20$ covalently bound to the SAM surface is shown in Figure 1.

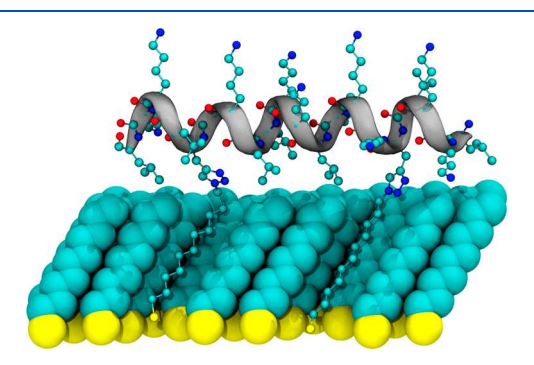


Figure 1. Three-dimensional illustration of α LK2x20 covalently bound to a decanethiol SAM by a 1,2,3-triazole ring formed between the terminal azides of the SAM and the propargylglycine residues of the peptide. The peptide backbone is shown as a gray ribbon, highlighting the α -helical secondary structure. The decanethiols of the SAM are shown as spheres. The peptide and the two covalently attached undecanethiols are shown in a ball-and-stick model. Atoms are colored by element: cyan, carbon; blue, nitrogen; red, oxygen; and yellow, sulfur. Hydrogens are omitted for clarity.

Neutron Reflectometry. Reflectivity measurements were completed on the Liquids Reflectometer, BL-4B, at Oak Ridge National Laboratory's (ORNL) Spallation Neutron Source. The Q range, 0.08-0.238 Å⁻¹, was attained by varying both the incident beam's angle (0.60-2.71°) and wavelength (2.50-16.75 Å) in seven intervals. Reflected neutrons were detected by the time-of-flight method on a two-dimensional position-sensitive ³He detector. Liquid experiments were completed using a custom liquid cell built and maintained at ORNL, which is described in detail elsewhere. 42 Samples were first measured under ambient conditions and then immersed in D₂O. After measurements in D₂O, the sample was removed from the cell and dried with clean $N_2(g)$. Finally, samples were measured while immersed in a 70/30 v/v D₂O/H₂O mixture. The D_2O/H_2O ratio was chosen because the scattering-length density (SLD) of this mixture was close to the SLD value of Au, which allowed the organic layers to be clearly distinguished from neighboring laminae. Prior to all liquid runs, the liquid cell was flushed with a volume 5 times that of the liquid cell before

NR measures the specular reflection of neutrons from thin film structures on a single-crystal Si substrate, which is a function of the chemical composition, thickness, and surface roughness of the SiO_{x} , Cr , Au , SAM , peptide, and water interfaces that comprise our films. Reflectivity was plotted with respect to Q, the wave transfer vector, to obtain reflectivity profiles for each data set. Q is the difference between absolute values of the initial wave vector, $k_{Q,Z}$, of the approaching beam and the final reflected wavevector, $k_{R,Z}$, and is calculated with eq 1

$$Q = \frac{4\pi \sin \theta}{\lambda} \tag{1}$$

where θ and λ are the angle of incidence and wavelength of incident neutrons, respectively. The wave vectors that define Q are illustrated in Figure 2.

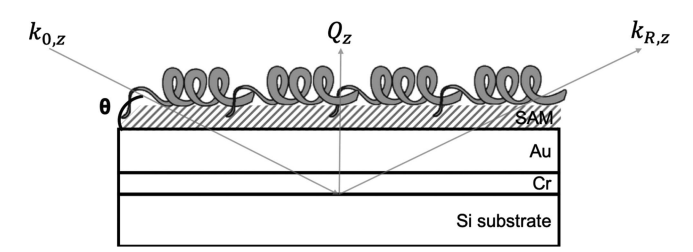


Figure 2. Schematic of an NR experiment conducted on α LK2x20-functionalized surfaces in air. Experiments completed in the liquid cell are described by an inverted version of this diagram. Layers are not depicted to scale.

Each sample's measured reflectivity was a function of the thickness, interfacial roughness, and SLD of every layer in each sample. The SLD is defined by eq 2

$$SLD = \frac{\sum b_i}{V_{\rm m}} \tag{2}$$

where b_i represents the scattering lengths (compiled by NIST) of every atom, i, in the molecular volume, $V_{\rm m}$. The SLD is a quantitative value for the isotopic composition and density and is therefore critical for measuring water in individual layers of the sample. For the peptide-functionalized system presented here, SLD changes of the peptide layer when in air, versus immersion in D₂O, versus immersed in a 70/30 v/v mixture of D₂O/H₂O provided direct physical evidence for how much water surrounded α LK2x20 on the SAM

NR data was modeled with ORNL's web interface for reflectivity fitting (Webi) created by Doucet et al., which uses NIST's REFL1D Python package. 45,46 Webi uses an iterative process to fit reflectivity using the Nelder-Mead and DREAM algorithms, which minimize χ^2 values within predefined boundaries. Boundaries for each parameter (thickness, SLD, and roughness) were chosen to preserve the physical relevance of each layer in the samples, which was determined using other analytical techniques or previously published values. First, the thickness, SLD, and roughness values for the SiO_v, Cr, and Au layers were modeled while allowing the SAM and peptide layers to vary widely. Solutions for each parameter of these layers were allowed to vary by up to 10% across the three different data sets to account for an expected 10% systematic error inherent in NR measurements obtained in different geometries. SiO_x thicknesses were well matched with those reported by ellipsometry prior to deposition (data not shown). Cr and Au thicknesses were closely representative of the thicknesses estimated by the deposition chamber's quartz crystal microbalance (QCM). SLD values for Cr and Au were constrained within 90 to 100% of published bulk values (Cr, $3.03 \times 10^{-6} \text{ Å}^{-2}$; Au, $4.6 \times 10^{-6} \text{ Å}^{-2}$. SLDs lower than reported bulk values were expected because of inevitable defects produced by this deposition method. The SLD of the Si substrate was held to the published bulk value of $2.067 \times 10^{-6} \text{ Å}^{-2}$, and the SLD of ambient air was set equal to 0. SLDs of bulk D_2O (6.36 \times 10⁻⁶ Å⁻²) and 70/30 v/v D_2O/H_2O (4.27 \times 10⁻⁶ Å⁻²) were not constrained, which permitted fits to determine an accurate SLD for each solvent. This was done because bulk D2O was prone to SLD impurities from absorbed ambient gases and small percentages of hydrogenation and the D2O/H2O mixture suffered from random volumetric errors. Consequently, the real SLDs varied from the theoretical values.

After the inorganic layers' thickness, SLD, and roughness values were established for each sample, the 25AzUDT and α LK2x20 layers were fit. Samples reported here were best fit to two separate layers for 25AzUDT and α LK2x20, as opposed to one layer that encompasses both 25AzUDT and α LK2x20. We have previously reported a detailed NR analysis of 25AzUDT both in air and immersed in water. ⁴² Best fits for the organic layers included thickness and SLD values reasonably close to our previous report while allowing for enough variation to include potential interactions with α LK2x20 side chains. Models for α LK2x20 were limited to those with thicknesses of less

than 30 Å because that is the approximate maximum height of the peptide when in a helical conformation and oriented perpendicular to the SAM surface.³⁷ Finally, additional confidence in the final fits came from models with closely matched thickness and SLD values across the three samples.

The water contribution in the 25AzUDT and α LK2x20 layers was calculated as N_{w} , the number of waters per thiol or peptide molecule, respectively, using eq 3,

$$N_{\rm w} = \frac{(S_{\rm E} \times V_{\rm m} - \sum b_{\rm L})}{\sum b_{\rm W}} \tag{3}$$

where $S_{\rm E}$ is the experimental SLD during immersion in water and $V_{\rm m}$ is the experimental molecular volume of the 25AzUDT or α LK2x20 layer. $\Sigma b_{\rm L}$ is the total scattering length of 25AzUDT or α LK2x20 and $\Sigma b_{\rm w}$ is the scattering length of water or heavy water. $\Sigma b_{\rm w}$ was determined by dividing the fit values of the SLD of the bulk solution by the bulk molecular volume of D_2 O (30.19 ų).

Molecular Dynamics Simulations. Analyses were performed on the MD trajectory reported previously.⁴¹ All analyses were performed using modules in the Gromacs 2016.3 molecular dynamics simulation package.^{48–54} Volumes were calculated using the gmx sasa module, hydrogen bonds were counted using the gmx hbond module, and nearby waters were calculated using the gmx select module. All further analyses were performed in Python. Images of MD snapshots were generated using the Visual Molecular Dynamics (VMD) software.⁵⁵

RESULTS AND DISCUSSION

Reflectivities of α LK2x20-functionalized surfaces were first measured in air, then immersed in D₂O, and finally measured in a 70/30 v/v mixture of D₂O/H₂O, which was chosen to contrast match the Au layer. Figure 3A is a representative

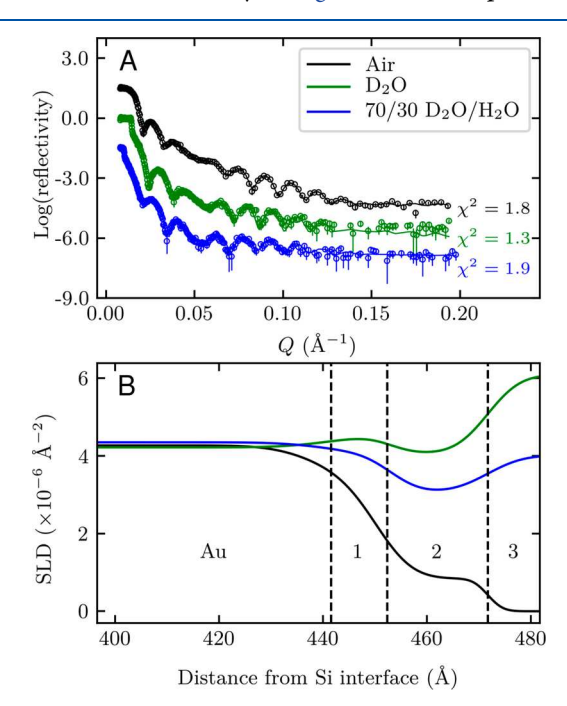


Figure 3. Representative NR data and Webi fits for α LK2x20 covalently attached to a SAM. (A) Collected reflectivity data (open circles) and best fit Webi models (solid lines) of the peptide-functionalized surfaces. The error bars represent the experimental error in reflectivity. Black, data collected in air; green, data collected in D₂O; and blue, data collected in 70/30 v/v D₂O/H₂O. Reflectivity profiles are offset along the y axis for clarity. (B) SLD profiles zoomed in on the interfaces of interest. Region 1, 25AzUDT; region 2, α LK2x20; region 3, environment of the sample (air or the aqueous solution).

Table 1. Average SLD and Thickness (t) Values among the Three Samples for the Organic Layers on Top of Au

layer	air SLD (× 10^{-6} Å ⁻²)	$D_2O SLD (\times 10^{-6} \text{ Å}^{-2})$	$70/30 \text{ D}_2\text{O}/\text{H}_2\text{O} \text{ SLD } (\times 10^{-6} \text{ Å}^{-2})$	air t (Å)	$D_2O\ t\ (\text{Å})$	$70/30 \ D_2O/H_2O \ t \ (Å)$
25AzUDT	3.25 (0.05)	4.4 (0.3)	3.9 (0.2)	11 (2)	12 (1)	11 (1)
α LK2x20	0.83 (0.01)	4.41 (0.04)	3.1 (0.1)	20.9 (0.3)	20 (3)	19 (3)
environment	0	6.09 (0.07)	4.06 (0.07)			

^aThe reported error in parentheses is the standard deviation of three replicates.

reflectivity profile of the raw reflectivity (empty circles) and experimental error (error bars) for a peptide-functionalized surface in air (black), D_2O (green), and $\tilde{D_2O}/H_2O$ (blue). The final Webi fits are shown as solid lines. From these fits, the SLD values for the interfaces of interest were graphed as a function of layer thickness in Figure 3B. This SLD profile provides a visual representation of how each layer's composition changed as a function of the environment, identified as region 1 (25AzUDT), region 2 (α LK2x20), and region 3 (air or the aqueous solution). The curvature of the transition from one SLD to another is representative of the roughness of the respective interface; a perfect monolayer with no roughness would result in a step transition from the SLD of one layer to the next. It is clear that when immersed in the isotopically contrasting water environments the SLD of 25AzUDT (region 1) and α LK2x20 (region 2) increased compared to the air environment, implying that water penetrated these layers to some extent. The individual fit values and respective model confidences for each sample are reported in Table S2. Fit confidences for the values used to determine structural or compositional changes (thickness and SLD) were <6%.

Analysis of the SAM in Air. It was important to have a physical understanding of the peptide and SAM layers in air prior to immersion in water in order to accurately quantify water around αLK2x20 and 25AzUDT. First, the inorganic layers (SiO_x, Cr, and Au) were modeled, which is discussed in detail in the Supporting Information. We previously reported that SAMs on Au surfaces deposited on Si of the same composition used here exhibit densities that are 68-76% of theoretical close-packed SAMs. The theoretical SLD of 25AzUDT is $5.46 \times 10^{-6} \text{ Å}^{-2}.^{42}$ At these densities, the SLD of 25AzUDT was expected to be in the range of $(3.6-4.1) \times$ 10^{-6} Å^{-2} . However, the average SLD and standard deviation of 25AzUDT in air among the three replicate samples here was $(3.25 \pm 0.05) \times 10^{-6} \text{ Å}^{-2}$ (Table 1). This SLD value represents 60% density coverage, which is at least 8% lower than the thiol density reported for this SAM prior to peptide functionalization. We considered three possible reasons the SAM SLD was decreased after peptide functionalization: (1) the NR models determined a different boundary between the SAM and peptide layer than between the SAM alone and air; (2) leucine side chains, which have negative scattering lengths, were penetrating the SAM; and (3) the SAM density was physically reduced by contact with the peptide, exposure to click reaction conditions, or both.

To examine the first reason listed above, we compared the thickness of 25AzUDT measured in this study, 11 ± 2 Å, to the previously measured thickness, 14.4 ± 0.3 Å. We attributed this difference to the way the models defined the boundary above the SAM; the interface between 25AzUDT and α LK2x20 was defined differently than that between 25AzUDT and air. For the peptide-functionalized surface, the remaining azide groups terminating the SAM and the triazole rings connecting 25AzUDT to α LK2x20 were

recognized as part of the peptide layer by the NR fit rather than 25AzUDT. Prior to peptide functionalization, azide groups were included in the SAM thickness value. Removing the nitrogen atoms from the calculation of the total scattering length of 25AzUDT reduced the theoretical SLD by 4% and the height by approximately 2.5 Å. We also considered the possibility that binding α LK2x20 caused the SAM to compress, leading to a smaller observed SAM thickness; however, compressed thiols would have a decreased molecular volume, resulting in an increased SLD (eq 2). Because the SLD decreased upon peptide functionalization, the observed height reduction was not a result of the SAM compressing. Instead, the combination of the reduced SAM height and decreased SAM SLD suggested that the NR model identified the boundary between the SAM and peptide as below the triazole and remaining azide nitrogen atoms, which is lower than the boundary of the SAM and air when measured prior to peptide functionalization. Thus, our first hypothesis did account for a portion of the observed SLD decrease.

The second possible reason for a decreased SAM SLD could be due to the leucine side chains on the SAM-facing side of α LK2x20 intercalating to some extent into 25AzUDT as a result of attractive hydrophobic interactions. Because of the uncertainty of the molecular volume of the leucine side chains (which depends on their exact configuration), the SLD value could not be exactly determined; however, we can estimate this value based on its chemical structure. Considering the two leucine γ and γ' methyl groups were physically most likely to penetrate the SAM, we estimated the $V_{\rm m}$ of each of the methyl groups as 1/6 of the $V_{\rm m}$ of liquid hexane (218 Å³). Each methyl had a scattering length of -4.6×10^{-5} Å, resulting in an SLD of -1.2×10^{-6} Å⁻². Using this estimated SLD, the reduction of the SAM SLD from 3.6 to $3.25 \times 10^{-6} \,\text{Å}^{-2}$ can be accounted for if 7% of the measured composition of 25AzUDT were leucine methyl groups. Intercalation of the leucine side chains beyond the methyl terminal groups would have further reduced the SAM SLD and was therefore unlikely. Physically, a 7% leucine-methyl composition of the SAM layer corresponded to 1 methyl group per 1.4 thiols and therefore 22.3 thiols for the 8 leucine side chains on each peptide. This value was close to the 20 thiols underneath each peptide previously estimated by reconstructing a geometric model of this same peptide-functionalized surface visualized in STM images.³⁸ In the STM images, the oblong shape attributed to individual α LK2x20 peptides produced a box with dimensions of \sim 30 Å \times ~20 Å, which, when overlaid with an accurately scaled diagram of close-packed thiols in a $(\sqrt{3} \times \sqrt{3})R30^{\circ}$ configuration with a thiol-to-thiol spacing of 5 Å, allowed us to estimate that each peptide covered approximately 20 thiols. The agreement between the simple geometric model obtained from STM images and the NR calculated leucine:thiol ratio suggests that the methyl groups of the leucine residues indeed permeated the SAM, contributing to a reduced SLD. However, the peptide dimensions constructed from STM images were a simple approximation subject to visual error as a result of

misidentifying the boundaries of the peptides and to smearing effects from scanning the STM tip across the surface. Additionally, it was sterically unfavorable for every single leucine to penetrate into the SAM when the peptide was completely helical. Nevertheless, the reduction of the SAM SLD after peptide functionalization can be attributed to some of the leucine side chains penetrating into the SAM. We will revisit this proposed interaction later in the text.

Finally, the third possibility we considered was that the density of the SAM was reduced due to structurally induced disorder from either 1) physical contact between the side chains of α LK2x20 and the SAM, or 2) damage to the integrity of the SAM caused by the conditions of the click reaction. These two causes are not mutually exclusive and could have both simultaneously contributed. First, any contact between the peptide side chains and the SAM surface would likely disrupt the close-packing thiols, increasing $V_{\rm m}$, and therefore decreasing the SAM SLD. This effect would have been exacerbated by any leucines that intercalated into the SAM. Additionally, alkyl thiol SAMs are susceptible to damage when exposed to oxidizing and reducing agents or to high heat. 56-60 Although alkyl thiol SAMs have been successfully used as a click reactant in many other reports, 61,62 exposure to the cycloaddition reaction conditions may have caused some thiol reduction or desorption, especially at defect sites. This in turn would lower the overall SAM SLD, consistent with our experimental observations.

Because all of the aforementioned scenarios are possible explanations of the observed reduction in SLD of the SAM layer, we concluded that the change in SLD is likely due to a combination of all three reasons: (1) the NR model classifying the SAM as only the aliphatic portion of 25AzUDT; (2) some leucine methyl groups intercalated into the SAM; and (3) a reduction in SAM density from both the peptide-induced disorder and the loss of some thiols as a result of the click reaction environment. Nevertheless, characterizing the SAM layer provided the basis for analyzing the peptide layer and ultimately for quantifying the amount of water around both the SAM and the peptide.

Analysis of α LK2x20 in Air. Previously, α LK2x20functionalized surfaces were extensively characterized with multiple analytical methods. From these studies, we confirmed that α LK2x20 was covalently bound to the SAM and was α helical when dry and immersed in water. 37,38,40,60,63 Additionally, minimal physisorbed peptide was detectable after rinsing the surfaces according to the protocol outlined in the Experimental Section. 38,60 These prior experiments also serve as a comparison with which to confirm the values of the Webi fits. Having characterized the inorganic and SAM layers, we subsequently examined the peptide layer thickness determined by the Webi fits of our reflectivity data. In air, the average thickness and standard deviation between samples of the peptide-functionalized surface was $20.9 \pm 0.3 \text{ Å}$ (Table 1). Ellipsometry estimated the combined SAM and peptide thickness in air to be $26 \pm 1 \text{ Å},^{40}$ and the combined height of the SAM + peptide layer determined by NR was 32 Å (Table 1). Considering that the optical constants assigned to the organic layers in the ellipsometry experiment were approximated to those of C2H4, which does not accurately describe the SAM or peptide, we concluded that our NRdetermined heights were reasonable. Moreover, a small percentage of peptides were likely bound only at one position as a result of competitive inhibition of other nearby peptides.

In a previous study, this same peptide was designed to bind at only one site by replacing one of click reactant residues with glycine, and after functionalization, the peptide was observed to sit approximately 45° to the surface normal. In the NR experiments described in this report, the heights determined by the Webi fit were a weighted average of the heights between $\alpha LK2x20$ bound at one site and $\alpha LK2x20$ bound at two sites, resulting in a measured thickness of the peptide layer that was slightly larger than the height of the peptide parallel to Au. Overall, the height of the peptide layer measured with NR was consistent with values previously measured using other analytical techniques.

The physical space occupied by each α LK2x20 was further explored by analyzing the molecular volume, $V_{\rm m}$, calculated by the reflectivity obtained in air under the assumption that no water is present around the peptide in this environment. Dividing the total scattering length of α LK2x20 by the SLD of the peptide layer (Table 1) produced a V_m of 5760 \pm 70 Å³. The total scattering length of α LK2x20 was $4.78 \times 10^{-3} \text{ Å}^{-1}$, which included 12 extra nitrogen atoms to account for the triazole rings and 2 azide groups remaining underneath the peptide. The number of remaining azides was determined by the geometric approximation of peptide coverage from previously reported STM images. The peptide packing density was estimated from the $V_{\rm m}$ using a rectangular prism with the height equal to the thickness determined by NR in ambient air (Table 1). This led to an experimental area of 277 \pm 5 Å² occupied by each peptide. In comparison, the area calculated using the geometric approximation of the peptide dimensions obtained from STM images was ~600 Å², twice that determined by NR. However, it is important to note that the area calculated from the STM images was a simple geometric assignment to an observed shape appearing to be a single peptide and prone to errors discussed above. 42 The area per peptide measured by NR was more quantitative and representative of the average space occupied by a single peptide across the entire surface.

Analysis of α LK2x20 in Water and Comparison to MD. Because determining the number of water molecules around the peptide was dependent on the peptide $V_{\rm m}$ remaining constant between environments (eq 3), it was important to revisit the thickness measured by NR for the peptide layer. The thickness values are shown in Table 1, and the errors in parentheses are the standard deviations of the layer heights between samples. However, it is relevant to note that these surfaces are not atomically flat and are instead intrinsically rough, meaning that the heights determined by NR should be interpreted as average heights and not absolute heights. The transition from bulk water to peptide and peptide to SAM was better described as a range in which the interfacial roughness was the RMS error of the thickness reported. The thickness and roughness values of the organic layers for each sample are reported in Table S2 for reference.

From Table 1, the observed peptide heights for immersion in D_2O ($20\pm3\,\text{Å}$) and $70/30\,D_2O/H_2O$ ($19\pm3\,\text{Å}$) were not statistically different from the thickness measured in ambient air ($20.9\pm0.3\,\text{Å}$). The $V_{\rm m}$ used for the peptide layer that was derived from the SLD of αLK2x20 in air is therefore applicable to calculating the quantity of water (using eq 3) around the peptide when immersed in aqueous environments. However, the experimentally measured thickness of the peptide in water must have also included any water molecules associated with the solution-facing side of the peptide, despite having a

statistically similar overall height of the peptide layer. Considering that one hydrogen-bound water associated with the top of the peptide accounts for approximately 4.7 Å, 65,66 we concluded that the atomic structure of α LK2x20 was compressed in the z direction (perpendicular to the SAM surface) after immersion in water, resulting in a height of the peptide structure itself of 14-15 Å. To test this apparent height, we consulted previously published MD simulations of a single α LK2x20 peptide on a decanethiol SAM in water. 41 In that report, we demonstrated that the simulations were able to accurately reproduce the experimentally observed secondary structure content of the peptide. These simulations therefore provided a source of atomistic insight into the NR-derived height measured in water. From the simulations, the number density profile of the peptide atoms along the z dimension of the simulation box was calculated and is shown in Figure 4A.

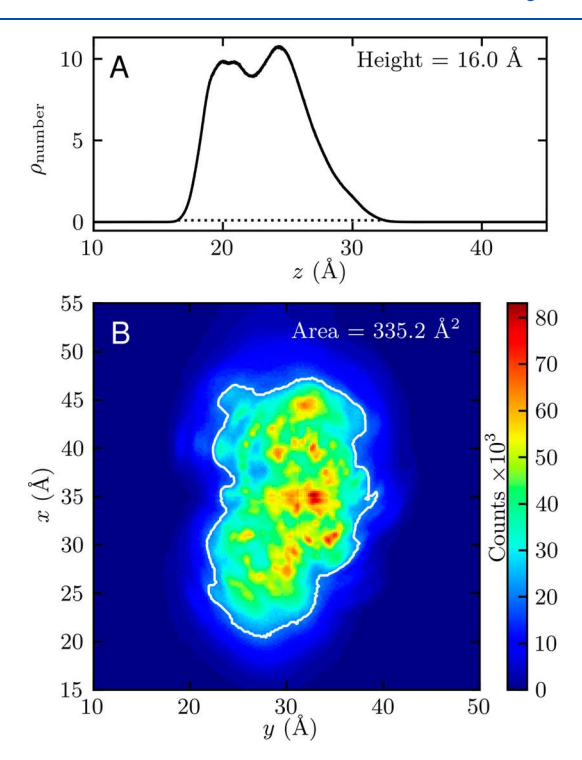


Figure 4. Dimensions of the α LK2x20 peptide estimated from MD simulations. (A) Number density profile (black trace) of the peptide atoms projected along the z dimension, where the bottom of the simulation box is set to zero. The height of the peptide (16.0 Å) was estimated by measuring the width of the profile (dotted line). (B) Intensity map of the positions of peptide atoms projected onto an x-y plane representing the SAM after the removal of the rotational and translational degrees of freedom. The white contour line represents 25% of the maximum count, and the area enclosed in this contour is 335.2 Å².

We estimated the height of the peptide to be 16 Å by measuring the width of the number density peak from this profile (horizontal dotted line). This is in close agreement with the estimated height of the α LK2x20 structure in water from the NR experiments and supports the conclusion that the peptide was compressed toward the SAM upon immersion in water.

We conclude that the height of the peptide in water that was compressed from 20.9 to 14–15 Å is compatible with the general expectation of the hydrophobic effect. In the presence of water, it is favorable for the leucines to collapse toward the

SAM to maximize water exclusion and create a hydrophobic peptide—surface interaction. In an ambient environment without water, the entropic driving force of the hydrophobic interaction is absent, which would allow the leucine residues to relax away from the surface, increasing the apparent height of the peptide above the surface. Ambient air molecules present during the NR experiment were nonpolar (primarily N_2 , O_2 , and CO_2) and would interact with the SAM to the same degree as the leucine residues. Given the evidence presented, we propose that the heights of $\alpha LK2x20$ -functionalized surfaces measured by NR were altered slightly by a "buoyancy" effect, where the peptide lifted away from the SAM in air on a layer of gas molecules and collapsed onto the SAM surface in an aqueous environment.

To compare the experimentally determined area occupied by each peptide to our MD simulations, we projected the position of the peptide atoms onto an x-y plane parallel to the SAM surface. The projected profile is shown in Figure 4B. The white contour line represents 25% of the maximum count, and therefore the majority of the sampled conformations fell within the contour. The area contained within the contour was calculated to be 335 ${\rm \AA}^2$, which was slightly larger than the experimental area of 277 ${\rm \AA}^2$ estimated by the NR experiments. This discrepancy was likely due to the fact that the MD simulations were of an isolated single peptide on the SAM while experimentally the peptides on the SAM surface were closely packed. Therefore, any conformational restrictions due to neighboring peptides were unaccounted for in the simulations. Additionally, the higher calculated area from MD could be the result of the harmonic restraints used to approximate the triazole linker groups, which likely overestimated the conformational flexibility of the peptide. The overestimation of the peptide area in simulation suggests that the positioning of the side chains and flexibility of the amide backbone were limited to the z axis in the experimental monolayer. Nevertheless, the area calculated from the MD simulations was reconcilable with the area observed from the NR experiments. Both of these values were significantly smaller than the area per peptide estimated by STM images, which were based on a simple geometric argument. The agreement between the MD simulations and NR experiments underscores the quantitative accuracy provided by this experimental

Quantifying Water Permeation in the SAM and Peptide Layers. With the SAM and peptide dimensions understood, the primary interest of the NR experiments was to quantify water associated with each component of the surface when submerged. In Figure 3B, the SLD traces diverge from a constant value at the interface of Au to 25AzUDT (region 1) and α LK2x20 (region 2), in which the changes in the SLDs of the organic layers were proportional to the environment's SLD (region 3). This directly indicated water uptake into both the SAM and peptide layers. The quantity of water in the SAM layer was calculated using eq 3, and these values are shown in Table 2, where N_w is the number of waters calculated per thiol or peptide. We formerly reported that 25AzUDT is prone to water penetration, with 1.6 water molecules associated with each thiol.⁴² In the present work, that amount doubled to an average of 2.7 ± 0.9 water molecules associated with each thiol after peptide functionalization. Taken in combination with the fact that the ambient SLD of 25AzUDT was also lower than expected, we hypothesized that the peptide structure disrupted the integrity of the SAM. As discussed previously, the

Table 2. Number of Waters per SAM Thiol or α LK2x20 Molecule^a

lay	rer	$N_{\rm W}$ D ₂ O	$N_{\rm W}~{\rm H_2O}$	average
25AzUDT		2.9 (0.7)	2.4 (0.6)	2.7 (0.9)
α LK2x20	100% H	113 (11)	109 (6)	111 (13)
	100% D	84 (11)	66 (6)	75 (13)

"Values for each environment are an average of all samples. The number of waters for $\alpha LK2x20$ was calculated for an entirely hydrogenated molecule (denoted as 100% H) and an entirely deuterium-exchanged molecule (denoted as 100% D). Errors reported in parentheses are the standard deviation values among the three replicate samples.

proximity of α LK2x20, the intercalation of its side chains, and the chemical environment of the click reaction all induced disorder in the close-packed domains of the thiols. The resulting disorder made the SAM more susceptible to water permeation despite its hydrophobicity. This is consistent with several studies that demonstrated that the apparent hydrophobicity of a SAM decreases with increased disorder. ^{29,67–70} Although it was unsurprising that a peptide placed on the surface disrupted the SAM structure, to the best of our knowledge this was the first direct measurement of this effect. This effect will likely influence the results other studies where SAMs are used to immobilize biological molecules and should not be ignored in any conclusions of protein structure on SAMs.

The amount of water surrounding α LK2x20 was calculated in the same manner as for 25AzUDT. However, there was uncertainty around the scattering length of the immersed peptide because, unlike the SAM, the peptide contained 51 exchangeable hydrogen atoms that could have been replaced with deuterium when immersed in the 2 heavy water environments: 3 from each of the 10 lysines, 19 from the amide backbone, and 2 from the N- and C-termini.71,72 Unfortunately, there was no way to accurately measure how many of the labile hydrogen atoms on α LK2x20 were replaced with deuterium during the aqueous NR experiments. Therefore, the number of waters surrounding each α LK2x20 was calculated for the two extreme cases: a fully hydrogenated peptide and a fully deuterated peptide. These are denoted in Table 2 as 100% H and 100% D, respectively. Assuming that the peptide was fully hydrogenated, we calculated 111 \pm 13 water molecules surrounding each peptide. Assuming that the peptide was fully deuterated, we calculated 75 \pm 13 water molecules surrounding each peptide. Because we are unable to determine the number of exchanged hydrogens, these two extremes define a range containing the true quantity of water around each peptide. This range of 75 to 111 waters is a substantial number of waters hydrating each peptide, despite the presence of the hydrophobic surface. We will return to this observation later.

To physically understand how this quantity of water interacts with the surface-bound peptide, we again referred to our previously published MD simulations. However, because the MD simulations were only of a single peptide on a SAM in a box of water, we needed to restrain our window of investigation to the physical values determined by NR: the range of the number of waters surrounding each peptide and the peptide molecular volume. To do this, we first calculated the number of water molecules near the peptide in the simulation as a function of an inclusion distance (d) away from

the peptide. These calculations are shown in Figure 5A, where the experimentally determined range of the number of waters

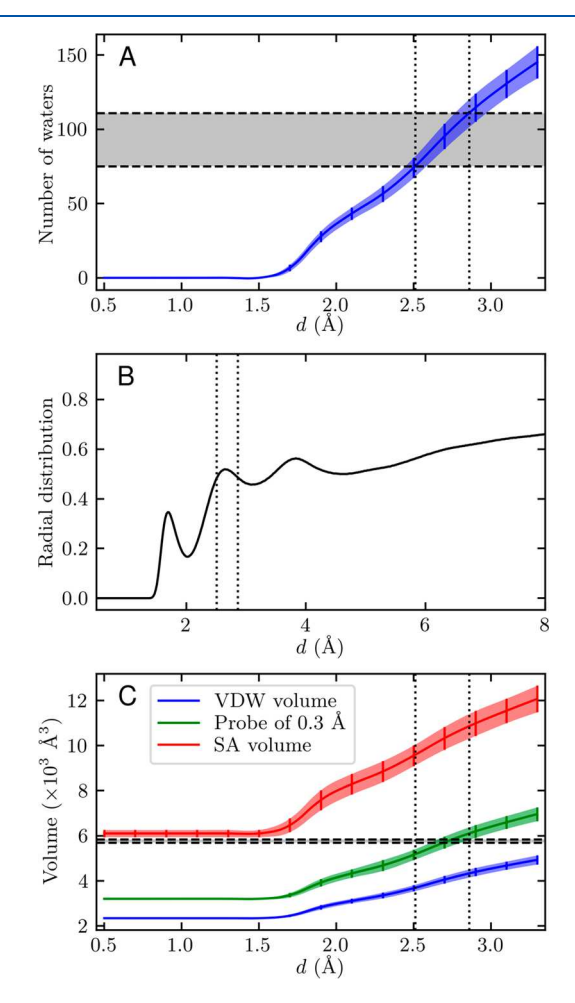


Figure 5. Comparison of the NR-determined number of waters and $V_{\rm m}$ to MD simulations. (A) Number of waters (y axis) within an inclusion distance (x axis) of the peptide averaged over a 1.25 μ s MD simulation. Error bars represent the standard deviation of the distribution of the water count. Horizontal dashed lines and the gray region represent the experimentally determined bounds for the number of waters in the peptide layer. Vertical dotted lines represent the bounds of the radii that have a water count within the experimental bounds and are interpolated from a spline fit to the data (solid curve). (B) Radial distribution function (RDF) between the heavy atoms of the protein and the oxygen atom of water molecules. Vertical dotted lines are reproduced from (A) and correspond to the minimum and maximum inclusion distances of water. Both cases contain the full first solvation peak. (C) Volume (y axis) encompassed by the peptide and waters within a certain inclusion distance, d (x axis), calculated with a 0 Å probe (blue), 0.3 Å probe (green), and 1.4 Å probe (red). The vertical dotted lines are reproduced from (A). The horizontal dashed lines and gray region represent the experimentally determined bounds of $V_{\rm m}$ of the peptide and water complex. Error bars represent the standard deviation of the distribution of the calculated volumes.

(from Table 2) is represented by the horizontal dashed lines. We then interpolated minimum and maximum inclusion distances of 2.51 and 2.86 Å, respectively (vertical dotted lines in Figure 5A), that corresponded to the minimum and maximum experimentally measured number of waters around each peptide (75 or 111 waters).

To understand the physical relevance of this amount of water, we plotted the radial distribution function (RDF) between the oxygen atoms of water and the heavy atoms of the peptide from the simulations (black trace in Figure 5B). Maxima in the RDF represent average distances between the peptide and water molecules in successive solvation shells. The α axis is the distance between any heavy atom of the protein and the oxygen atoms of water molecules.

To directly compare the x axis in Figure 5B to the inclusion distances determined in Figure 5A, we shifted the RDF along the x axis by subtracting 1.05 Å (the average hydrogen to heavy atom bond length) to account for the bond lengths of heavy atoms to hydrogens on the protein. We then reproduced the interpolated inclusion distances from Figure 5A, which corresponded to the minimum and maximum water quantities determined from the NR experiment, on Figure 5B (dotted vertical lines). For both the minimum and maximum cases, the entirety of the first solvation shell and part of the second solvation shell of water were within the corresponding distances. This indicated that the observed SLD of the peptide layer in water included the peptide encompassed by at least the full first solvation shell.

We next asked if the volume occupied by both the water and the peptide was consistent with the experimentally observed volume, $V_{\rm m}$, from the NR data. However, interpreting the experimental, surface-averaged V_{m} at an atomic level with MD is challenging because the corresponding volume definition for MD is ambiguous. For example, the volume contained within the van der Waals radii of the atoms in α LK2x20 does not account for the excluded volume inaccessible to solvent molecules, but the experimentally determined $V_{\rm m}$ contained the volume of this void space, the volume of the peptide itself, and the volume of the water molecules. Alternatively, calculating the volume enclosed by the solvent-accessible surface area of the peptide accounts for any void space volume inaccessible to a probe of radius 1.4 Å (the standard probe size used to represent the radius of water). These two calculations, referred to here as the vdW volume and the SA volume, are the volume extremes representable by a set of atoms. For each step of the MD simulation, the peptide and nearby water molecules with at least one atom within the inclusion distance, d, were extracted, and then the vdW volume and the SA volume were calculated for each of the extracted peptide-plus-water structures. The resulting volumes as a function of inclusion distance are shown in Figure 5C. The vertical dotted lines indicate the interpolated range of inclusion distances that corresponded to the range of water molecules determined from the NR experiment (2.51 and 2.86 Å as determined from Figure 5A). The horizontal dashed lines indicate the confidence interval of the experimentally determined $V_{\rm m}$. Therefore, the region within these four lines represents a $V_{\rm m}$ and water quantity that are consistent with the experimentally determined values. From this, it is clear that the vdW calculation (Figure 5C, blue trace) underestimated the molecular volume of the peptide, while the SA overestimated it (Figure 5C, red trace). To further investigate, we calculated the volume enclosed by the surface accessible to probes with a range of radii, from a probe radius of 0.0 Å (which is equivalent to the vdW volume) to 1.4 Å (which is equivalent to the SA volume). We found that a probe radius of 0.3 Å resulted in an enclosed volume of $5710 \pm 260 \text{ Å}^3$, consistent with the best fits to the NR data. Within this volume there were 95 \pm 8 waters, which corresponded to the first solvation shell of the peptide

(Figure 5B) and was in the middle of the range calculated by NR (Table 2). Considering previous STM images revealed that the peptides were close packed on the surface, the NR fits and the simulation data together imply that the packing of $\alpha LK2x20$ on the surface contains enough space between peptides to include at least a single full solvation shell around each peptide.

Having found parameters describing the amount and volume of water present around the peptide that were consistent with the NR experimental data, we visualized the placement of individual water molecules around the peptide using snapshots from the MD simulation. Figure 6 illustrates a representative

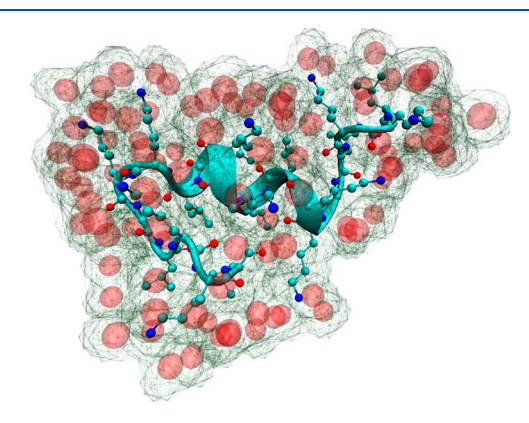


Figure 6. Representative snapshot from the MD simulations with 96 water molecules (red spheres) and a $V_{\rm m}$ of 5770 ų. The SAM surface is in the plane of the page. The excluded volume (calculated using the 0.3 Å probe determined in Figure 5) is contained within the transparent green wire surface. The peptide backbone is shown as a cyan ribbon, and the heavy atoms of the side chains are represented with a ball-and-stick model.

snapshot of α LK2x20, where the peptide is oriented such that the SAM surface is in the plane of the page. All water molecules within 2.7 Å of the peptide are represented by red spheres centered on the oxygen atoms. The particular snapshot shown had 96 water molecules in an excluded volume of 5770 Å³, consistent with the experimental limits determined from fitting the NR results. The volume is contained within the transparent green surface, which was calculated using a 0.3 Å probe as discussed above. Although the hydrogen atoms were removed for visual clarity, we observed several water molecules that were hydrogen bound to the side chains of lysine residues, as expected for solvent-exposed lysines. Even at the hydrophobic leucine/SAM interface, there was enough solventaccessible volume to allow for water penetration and interaction. Surprisingly, we also observed hydrogen bonds between water and the amide backbone of the leucine residue despite the proximity of the hydrophobic surface. These hydrogen bonds were particular to residues that were in a nonhelical conformation. We interpreted this observation to indicate that water-amide hydrogen bonds compete with hydrogen bonding along the peptide backbone, destabilizing the secondary structure.

Because of the importance of hydrogen-bonded waters in the stability of secondary structures in other systems, we quantified the extent of hydrogen bonding to the peptide (Figure 7). On average, 49 \pm 5 waters were hydrogen bound to the peptide, which accounts for 51% of the total number of waters observed within the average 5710 Å 3 $V_{\rm m}$ in the MD simulations. To put this in perspective, we compared the level

1

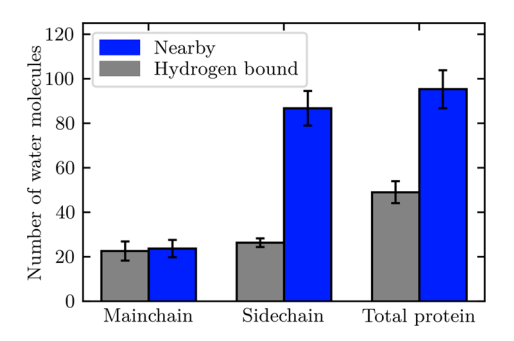


Figure 7. Number of waters interacting with α LK2x20 in our MD simulations. (Dark blue) Number of water molecules within the 2.7 Å inclusion distance. (Gray) Average number of observed hydrogenbonding water molecules. Error bars represent standard deviations of the distribution of the water molecule count.

of solvation of the peptide on the hydrophobic SAM surface to the level of solvation of the peptide free in solution. Because this particular sequence of peptide rapidly unfolds in aqueous solution, a direct comparison to the amount of water surrounding a helical fold of this peptide while dissolved in water was not possible. Instead, the peptide in water assumes a largely disordered, random coil structure, which we have shown in our previous experiments and MD simulations. From these simulations, we measured the number of water molecules within the same inclusion distance (3.3 Å) to be 200 \pm 11. Thus, there was roughly half of the amount of water surrounding the folded peptide bound to the SAM surface compared to the peptide completely dissolved in water.

However, there was only an ~20% decrease in water directly hydrogen bound to the peptide. The unfolded peptide in solution had 61 ± 4 waters hydrogen bound, whereas the peptide folded on the SAM surface had 49 \pm 5. In the simulations, the SAM-bound peptide had an average of 6 amino acids participating in intramolecular hydrogen bonding to form a helical structure, corresponding to a loss of 12 available hydrogen bonding functional groups. Therefore, the ~20% decrease in hydrogen-bound waters from the unfolded peptide in water compared to the folded peptide on the SAM could be attributed to the change in secondary structure of the peptide rather than the presence of the hydrophobic SAM. This observation reveals the crucial role of water in stabilizing or destabilizing secondary structure, even at hydrophobic interfaces. There was a significant amount of water accessible to the peptide in the presence of the hydrophobic SAM. This raises the following question: what facilitates protein hydration at protein-surface interfaces? Although there is evidence suggesting that surface hydration contributes to protein adsorption or repulsion, 73-75 experiments measuring protein hydration during adsorption as well as at steady state could provide significant insight into the hydration mechanism at abiological surfaces. Future SFG and MD studies will play a critical role in answering this question.

Overall, the results presented here show that α LK2x20 covalently bound to 25AzUDT was highly accessible to water molecules. One consideration for the significant amount of water measured, even along the amide backbone of the peptide at the hydrophobic interface, is that the covalent triazole bond restricted the conformational space available to the peptide, particularly on the hydrophobic side of the peptide (facing the SAM). In the absence of this covalent restraint, this peptide may have condensed even further into the SAM to maximize

hydrophobic interactions, changing the available space for water. This constriction of peptide conformational space and available water could explain why some proteins are stabilized when covalently linked to surfaces but not when adsorbed. The exact level of protein solvation, which can be quantitatively and directly measured at surfaces using the methods described here, likely plays a critical role in the stability of the structure. Such a hypothesis leads to future work measuring the amount of water associated with peptides adsorbed to SAMs instead of covalently tethered to inorganic surfaces. Additionally, future SFG experiments can measure changes in peptide and SAM structure in order to assess the extent that peptides are able to condense into the SAM when covalently bound versus adsorbed.

CONCLUSIONS

Structural water is known to play an important role in the stability of protein structure and therefore in determining the location and abundance of water at a protein-surface interface, which is paramount to understanding the destabilization of proteins upon immobilization. Using NR experiments, we quantified the amount of water surrounding an amphiphilic α helical peptide, aLK2x20, covalently attached to a SAM surface. We found that the integrity of the SAM was disrupted by α LK2x20, creating space that allowed twice as much water to penetrate the SAM when compared to SAMs prior to functionalization. Furthermore, we found that between 75 and 111 water molecules surrounded each peptide when submerged in an aqueous environment. By comparing the NR experiments to previously published MD simulations, we demonstrated that these water molecules comprised the entire first solvation shell of the peptide, indicating that the immobilized peptide had access to sufficient water to impact its secondary structure. Half of these water molecules were hydrogen bound directly to the peptide, including many to the amide backbone despite the presence of the underlying hydrophobic surface. Finally, comparing the NR results of the peptide in water versus the peptide in air suggested that αLK2x20 compressed into the SAM when immersed in solution, an effect likely driven by hydrophobic interactions and water exclusion, and experienced a buoyancy effect when in air. Overall, these results provide a quantitative, atomistic observation of the relationship between water and a peptide covalently immobilized onto a surface. These experiments present a framework for determining how much water is accessible to biomolecules, such as full proteins, covalently bound to similar surfaces. Ultimately, such experiments will provide insight into the role of water in stabilizing or destabilizing these structures.

ASSOCIATED CONTENT

Supporting Information

The Supporting Information is available free of charge at https://pubs.acs.org/doi/10.1021/acs.langmuir.9b02559.

Table listing the thickness, SLD, and roughness of SiO_x, Cr, and Au values for each sample from all three sample environments; reflectivity profiles, Webi fits, and SLD profiles of two of the three replicates (PDF)

AUTHOR INFORMATION

Corresponding Author

*E-mail: lwebb@cm.utexas.edu.

ORCID ®

Jeremy T. First: 0000-0001-8829-280X Mathieu Doucet: 0000-0002-5560-6478 Lauren J. Webb: 0000-0001-9999-5500

Present Address

¹Sandia National Laboratories, Albuquerque, New Mexico 87123, United States.

Author Contributions

These authors contributed equally.

Notes

The authors declare no competing financial interest.

ACKNOWLEDGMENTS

The work reported here was supported by the National Science Foundation (grant no. CHE-1807215). A portion of this research used resources at the Spallation Neutron Source, a DOE Office of Science User Facility operated by the Oak Ridge National Laboratory. The research at Oak Ridge National Laboratory's Spallation Neutron Source was sponsored by the Scientific User Facilities Division, the Office of Basic Energy Sciences, and the U.S. Department of Energy. The authors are thankful for the instrumentation available through the Texas Materials Institute at the University of Texas at Austin. We acknowledge the Texas Advanced Computing Center at The University of Texas at Austin for providing high-performance computing resources that have contributed to the results reported here. Sandia National Laboratories is a multimission laboratory managed and operated by National Technology & Engineering Solutions of Sandia, LLC, a wholly owned subsidiary of Honeywell International Inc., for the U.S. Department of Energy's National Nuclear Security Administration under contract DE-NA0003525. This article describes objective technical results and analysis. Any subjective views or opinions that might be expressed in the paper do not necessarily represent the views of the U.S. Department of Energy or the United States Government.

REFERENCES

- (1) Nel, A. E.; Mädler, L.; Velegol, D.; Xia, T.; Hoek, E. M. V; Somasundaran, P.; Klaessig, F.; Castranova, V.; Thompson, M. Understanding Biophysicochemical Interactions at the Nano–Bio Interface. *Nat. Mater.* **2009**, *8*, 543–557.
- (2) Rodriguez-Quijada, C.; Sánchez-Purrà, M.; de Puig, H.; Hamad-Schifferli, K. Physical Properties of Biomolecules at the Nanomaterial Interface. *J. Phys. Chem. B* **2018**, *122*, 2827–2840.
- (3) Nöll, T.; Nöll, G. Strategies for "Wiring" Redox-Active Proteins to Electrodes and Applications in Biosensors, Biofuel Cells, and Nanotechnology. *Chem. Soc. Rev.* **2011**, *40* (7), 3564–3576.
- (4) Willner, B.; Katz, E.; Willner, I. Electrical Contacting of Redox Proteins by Nanotechnological Means. *Curr. Opin. Biotechnol.* **2006**, 17 (6), 589–596.
- (5) Schneider, E.; Clark, D. S. Cytochrome P450 (CYP) Enzymes and the Development of CYP Biosensors. *Biosens. Bioelectron.* **2013**, 39 (1), 1–13.
- (6) Kienle, D. F.; Falatach, R. M.; Kaar, J. L.; Schwartz, D. K. Correlating Structural and Functional Heterogeneity of Immobilized Enzymes. *ACS Nano* **2018**, *12* (8), 8091–8103.
- (7) Limo, M. J.; Sola-Rabada, A.; Boix, E.; Thota, V.; Westcott, Z. C.; Puddu, V.; Perry, C. C. Interactions between Metal Oxides and Biomolecules: From Fundamental Understanding to Applications. *Chem. Rev.* **2018**, *118* (22), 11118–11193.
- (8) Bellissent-Funel, M. C.; Hassanali, A.; Havenith, M.; Henchman, R.; Pohl, P.; Sterpone, F.; Van Der Spoel, D.; Xu, Y.; Garcia, A. E.

Water Determines the Structure and Dynamics of Proteins. Chem. Rev. 2016, 116 (13), 7673-7697.

- (9) Kuntz, I. D.; Kauzmann, W. Hydration of Proteins and Polypeptides. *Adv. Protein Chem.* **1974**, 28, 239–345.
- (10) Kuntz, I. D. Hydration of Macromolecules. III. Hydration of Polypeptides. J. Am. Chem. Soc. 1971, 93 (2), 514-516.
- (11) Lu, J.; Su, T.; Thirtle, P.; Thomas, R.; Rennie, A.; Cubitt, R. The Denaturation of Lysozyme Layers Adsorbed at the Hydrophobic Solid/Liquid Surface Studied by Neutron Reflection. *J. Colloid Interface Sci.* 1998, 206 (1), 212–223.
- (12) Guo, S.; Pranantyo, D.; Kang, E. T.; Loh, X. J.; Zhu, X.; Jańczewski, D.; Neoh, K. G. Dominant Albumin-Surface Interactions under Independent Control of Surface Charge and Wettability. *Langmuir* 2018, 34 (5), 1953–1966.
- (13) Roach, P.; Farrar, D.; Perry, C. C. Interpretation of Protein Adsorption: Surface-Induced Conformational Changes. *J. Am. Chem. Soc.* **2005**, *127* (22), 8168–8173.
- (14) Zerze, G. H.; Mullen, R. G.; Levine, Z. A.; Shea, J. E.; Mittal, J. To What Extent Does Surface Hydrophobicity Dictate Peptide Folding and Stability near Surfaces? *Langmuir* **2015**, *31* (44), 12223–12230.
- (15) Langdon, B. B.; Kastantin, M.; Schwartz, D. K. Apparent Activation Energies Associated with Protein Dynamics on Hydrophobic and Hydrophilic Surfaces. *Biophys. J.* **2012**, *102* (11), 2625–2633
- (16) Sola-Rabada, A.; Michaelis, M.; Oliver, D. J.; Roe, M. J.; Colombi Ciacchi, L.; Heinz, H.; Perry, C. C. Interactions at the Silica—Peptide Interface: Influence of the Extent of Functionalization on the Conformational Ensemble. *Langmuir* **2018**, 34 (28), 8255—8263.
- (17) McUmber, A. C.; Randolph, T. W.; Schwartz, D. K. Electrostatic Interactions Influence Protein Adsorption (but Not Desorption) at the Silica—Aqueous Interface. *J. Phys. Chem. Lett.* **2015**, *6* (13), 2583—2587.
- (18) Todorovic, S.; Jung, C.; Hildebrandt, P.; Murgida, D. H. Conformational Transitions and Redox Potential Shifts of Cytochrome P450 Induced by Immobilization. *JBIC, J. Biol. Inorg. Chem.* **2006**, *11* (1), 119–127.
- (19) Deshapriya, I. K.; Kumar, C. V. Nanobio Interfaces: Charge Control of Enzyme/Inorganic Interfaces for Advanced Biocatalysis. *Langmuir* **2013**, 29 (46), 14001–14016.
- (20) Thom, I.; Buck, M. On the Interpretation of Multiple Waves in Cyclic Voltammograms of Self-Assembled Monolayers of n-Alkane Thiols on Gold. Z. Phys. Chem. 2008, 222, 739–754.
- (21) Tanaka, M.; Hayashi, T.; Morita, S. The Roles of Water Molecules at the Biointerface of Medical Polymers. *Polym. J.* **2013**, *45* (7), 701–710.
- (22) Takano, K.; Yamagata, Y.; Funahashi, J.; Hioki, Y.; Kuramitsu, S.; Yutani, K. Contribution of Intra- and Intermolecular Hydrogen Bonds to the Conformational Stability of Human Lysozyme. *Biochemistry* **1999**, 38 (39), 12698–12708.
- (23) Meyer, E. Internal Water Molecules and H-bonding in Biological Macromolecules: A Review of Structural Features with Functional Implications. *Protein Sci.* 1992, 1 (12), 1543–1562.
- (24) Pal, S. K.; Peon, J.; Bagchi, B.; Zewail, A. H. Biological Water: Femtosecond Dynamics of Macromolecular Hydration. *J. Phys. Chem. B* **2002**, *106* (48), 12376–12395.
- (25) Clark, D. S.; Ball, P.; Littlechild, J. A.; Rice, D. W.; Halle, B. Characteristics of Nearly Dry Enzymes in Organic Solvents: Implications for Biocatalysis in the Absence of Water. *Philos. Trans. R. Soc., B* **2004**, 359 (1448), 1299–1307.
- (26) Ravindra, R.; Zhao, S.; Gies, H.; Winter, R. Protein Encapsulation in Mesoporous Silicate: The Effects of Confinement on Protein Stability, Hydration, and Volumetric Properties. *J. Am. Chem. Soc.* **2004**, 126 (39), 12224–12225.
- (27) Roy, S.; Covert, P. A.; FitzGerald, W. R.; Hore, D. K. Biomolecular Structure at Solid–Liquid Interfaces As Revealed by Nonlinear Optical Spectroscopy. *Chem. Rev.* **2014**, *114* (17), 8388–8415.

(28) Hopkins, A. J.; McFearin, C. L.; Richmond, G. L. SAMs under Water: The Impact of Ions on the Behavior of Water at Soft Hydrophobic Surfaces. *J. Phys. Chem. C* **2011**, *115* (22), 11192–11203

- (29) Tyrode, E.; Liljeblad, J. F. D. Water Structure Next to Ordered and Disordered Hydrophobic Silane Monolayers: A Vibrational Sum Frequency Spectroscopy Study. *J. Phys. Chem. C* **2013**, *117* (4), 1780–1790.
- (30) Leng, C.; Hung, H.-C.; Sun, S.; Wang, D.; Li, Y.; Jiang, S.; Chen, Z. Probing the Surface Hydration of Nonfouling Zwitterionic and PEG Materials in Contact with Proteins. *ACS Appl. Mater. Interfaces* **2015**, 7 (30), 16881–16888.
- (31) Pawlowska, N. M.; Fritzsche, H.; Blaszykowski, C.; Sheikh, S.; Vezvaie, M.; Thompson, M. Probing the Hydration of Ultrathin Antifouling Organosilane Adlayers Using Neutron Reflectometry. *Langmuir* **2014**, *30* (5), 1199–1203.
- (32) Tarasevich, B. J.; Perez-Salas, U.; Masica, D. L.; Philo, J.; Kienzle, P.; Krueger, S.; Majkrzak, C. F.; Gray, J. L.; Shaw, W. J. Neutron Reflectometry Studies of the Adsorbed Structure of the Amelogenin, LRAP. *J. Phys. Chem. B* **2013**, *117* (11), 3098–3109.
- (33) Perez-Salas, U. A.; Faucher, K. M.; Majkrzak, C. F.; Berk, N. F.; Krueger, S.; Chaikof, E. L. Characterization of a Biomimetic Polymeric Lipid Bilayer by Phase Sensitive Neutron Reflectometry. *Langmuir* **2003**, *19* (19), 7688–7694.
- (34) Delcea, M.; Krastev, R.; Gutberlet, T.; Pum, D.; Sleytr, U. B.; Toca-Herrera, J. L. Thermal Stability, Mechanical Properties and Water Content of Bacterial Protein Layers Recrystallized on Polyelectrolyte Multilayers. *Soft Matter* **2008**, *4* (7), 1414–1421.
- (35) Xue, Y.; He, L.; Middelberg, A. P. J.; Mark, A. E.; Poger, D. Determining the Structure of Interfacial Peptide Films: Comparing Neutron Reflectometry and Molecular Dynamics Simulations. *Langmuir* **2014**, *30* (33), 10080–10089.
- (36) DeGrado, W.; Lear, J. Induction of Peptide Conformation at Apolar Water Interfaces. 1. A Study with Model Peptides of Defined Hydrophobic Periodicity. *J. Am. Chem. Soc.* **1985**, *107* (10), 7684–7689.
- (37) Gallardo, I. F.; Webb, L. J. Demonstration of α -Helical Structure of Peptides Tethered to Gold Surfaces Using Surface Infrared and Circular Dichroic Spectroscopies. *Langmuir* **2012**, 28 (7), 3510–3515.
- (38) Raigoza, A. F.; Webb, L. J. Molecularly Resolved Images of Peptide-Functionalized Gold Surfaces by Scanning Tunneling Microscopy. *J. Am. Chem. Soc.* **2012**, *134* (47), 19354–19357.
- (39) Raigoza, A. F.; Onyirioha, K.; Webb, L. J. Controlling Noncovalent Interactions between a Lysine-Rich Alpha-Helical Peptide and Self-Assembled Monolayers of Alkanethiols on Au through Functional Group Diversity. *Appl. Surf. Sci.* **2017**, *396*, 1831–1839.
- (40) Gallardo, I. F.; Webb, L. J. Tethering Hydrophobic Peptides to Functionalized Self-Assembled Monolayers on Gold through Two Chemical Linkers Using the Huisgen Cycloaddition. *Langmuir* **2010**, 26 (24), 18959–18966.
- (41) First, J. T.; Webb, L. J. Agreement between Experimental and Simulated Circular Dichroic Spectra of a Positively Charged Peptide in Aqueous Solution and on Self-Assembled Monolayers. *J. Phys. Chem. B* **2019**, *123* (21), 4512–4526.
- (42) Fies, W.; Dugger, J. W.; Dick, J. E.; Wilder, L.; Browning, K.; Doucet, M.; Browning, J. F.; Webb, L. J. Direct Measurement of Water Permeation in Submerged Alkyl Thiol Self- Assembled Monolayers on Gold Surfaces Revealed by Neutron Reflectometry. *Langmuir* **2019**, *35*, 5647–5662 Article.
- (43) Zhang, S.; Maidenberg, Y.; Luo, K.; Koberstein, J. T. Adjusting the Surface Areal Density of Click-Reactive Azide Groups by Kinetic Control of the Azide Substitution Reaction on Bromine-Functional SAMs. *Langmuir* **2014**, *30* (21), 6071–6078.
- (44) Sears, V. F. Neutron Scattering Lengths and Cross Sections. *Neutron News* **1992**, 3 (3), 26–37.
- (45) Kienzle, P. A.; O'Donovan, K. V.; Ankner, J. F.; Berk, N. F.; Majkrzak, C. F. REFL1D https://github.com/reflectometry/refl1d.

(46) Doucet, M.; Ferraz Leal, R. M.; Hobson, T. C. Web Interface for Reflectivity Fitting. *SoftwareX* **2018**, *7*, 287–293.

- (47) Kell, G. S. Effects of Isotopic Composition, Temperature, Pressure, and Dissolved Gases on the Density of Liquid Water. *J. Phys. Chem. Ref. Data* **1977**, 6 (4), 1109–1131.
- (48) Abraham, M. J.; Murtola, T.; Schulz, R.; Páll, S.; Smith, J. C.; Hess, B.; Lindah, E. Gromacs: High Performance Molecular Simulations through Multi-Level Parallelism from Laptops to Supercomputers. *SoftwareX* **2015**, *1*–2, 19–25.
- (49) Berendsen, H. J. C.; van der Spoel, D.; van Drunen, R. GROMACS: A Message-Passing Parallel Molecular Dynamics Implementation. *Comput. Phys. Commun.* **1995**, *91* (1), 43–56.
- (50) Lindahl, E.; Hess, B.; Van Der Spoel, D. Package for Molecular Simulation and Trajectory Analysis. *J. Mol. Model.* **2001**, *7*, 306–317.
- (51) Van Der Spoel, D.; Lindahl, E.; Hess, B.; Groenhof, G.; Mark, A. E.; Berendsen, H. J. C. GROMACS: Fast, Flexible, and Free. *J. Comput. Chem.* **2005**, 26 (16), 1701–1718.
- (52) Hess, B.; Kutzner, C.; van der Spoel, D.; Lindahl, E. GROMACS 4: Algorithms for Highly Efficient, Load-Balanced, and Scalable Molecular Simulation. *J. Chem. Theory Comput.* **2008**, *4* (3), 435–447.
- (53) Pronk, S.; Páll, S.; Schulz, R.; Larsson, P.; Bjelkmar, P.; Apostolov, R.; Shirts, M. R.; Smith, J. C.; Kasson, P. M.; van der Spoel, D.; et al. GROMACS 4.5: A High-Throughput and Highly Parallel Open Source Molecular Simulation Toolkit. *Bioinformatics* 2013, 29 (7), 845–854.
- (54) Páll, S.; Abraham, M. J.; Kutzner, C.; Hess, B.; Lindahl, E. Tackling Exascale Software Challenges in Molecular Dynamics Simulations with GROMACS. *Lect. Notes Comput. Sci.* **2015**, 8759, 3–27.
- (55) Humphrey, W.; Dalke, A.; Schulten, K. VMD: Visual Molecular Dynamics. *J. Mol. Graphics* **1996**, *14* (1), 33–38.
- (56) Vericat, C.; Vela, M. E.; Corthey, G.; Pensa, E.; Cortés, E.; Fonticelli, M. H.; Ibañez, F.; Benitez, G. E.; Carro, P.; Salvarezza, R. C. Self-Assembled Monolayers of Thiolates on Metals: A Review Article on Sulfur-Metal Chemistry and Surface Structures. *RSC Adv.* **2014**, *4*, 27730–27754.
- (57) Love, J. C.; Estroff, L. A.; Kriebel, J. K.; Nuzzo, R. G.; Whitesides, G. M. Self-Assembled Monolayers of Thiolates on Metals as a Form of Nanotechnology. *Chem. Rev.* **2005**, *105* (4), 1103–1169.
- (58) Flynn, N. T.; Tran, T. N. T.; Cima, M. J.; Langer, R. Long-Term Stability of Self-Assembled Monolayers in Biological Media. *Langmuir* **2003**, *19* (26), 10909–10915.
- (59) Ulman, A. Formation and Structure of Self-Assembled Monolayers. Chem. Rev. 1996, 96 (4), 1533–1554.
- (60) Raigoza, A. F.; Fies, W. A.; Lim, A.; Onyirioha, K.; Webb, L. J. One-Pot Reaction for the Preparation of Biofunctionalized Self-Assembled Monolayers on Gold Surfaces. *Appl. Surf. Sci.* **2017**, 394, 288–296.
- (61) Collman, J. P.; Devaraj, N. K.; Chidsey, C. E. D. Clicking" Functionality onto Electrode Surfaces. *Langmuir* **2004**, 20 (4), 1051–1053.
- (62) Decréau, R. A.; Collman, J. P.; Hosseini, A. Electrochemical Applications. How Click Chemistry Brought Biomimetic Models to the next Level: Electrocatalysis under Controlled Rate of Electron Transfer. *Chem. Soc. Rev.* **2010**, 39 (4), 1291–1301.
- (63) Wilder, L. M.; Fies, W. A.; Rabin, C.; Webb, L. J.; Crooks, R. M. Conjugation of an α Helical Peptide to the Surface of Gold Nanoparticles. *Langmuir* **2019**, 35 (9), 3363–3371.
- (64) Raigoza, A. F.; Dugger, J. W.; Webb, L. J. Review: Recent Advances and Current Challenges in Scanning Probe Microscopy of Biomolecular Surfaces and Interfaces. ACS Appl. Mater. Interfaces 2013, 5 (19), 9249–9261.
- (65) Soper, A. K.; Benmore, C. J. Quantum Differences between Heavy and Light Water. *Phys. Rev. Lett.* **2008**, *101* (6), 65502.
- (66) Zhang, Y.; Xu, Z. Atomic Radii of Noble Gas Elements in Condensed Phases. Am. Mineral. 1995, 80 (7–8), 670–675.

(67) Lane, J. M. D.; Chandross, M.; Lorenz, C. D.; Stevens, M. J.; Grest, G. S. Water Penetration of Damaged Self-Assembled Monolayers. *Langmuir* **2008**, 24 (11), 5734–5739.

- (68) Dallin, B. C.; Yeon, H.; Ostwalt, A. R.; Abbott, N. L.; Van Lehn, R. C. Molecular Order Affects Interfacial Water Structure and Temperature-Dependent Hydrophobic Interactions between Nonpolar Self-Assembled Monolayers. *Langmuir* **2019**, *35*, 2078–2088.
- (69) Yeon, H.; Wang, C.; Van Lehn, R. C.; Abbott, N. L. Influence of Order within Nonpolar Monolayers on Hydrophobic Interactions. *Langmuir* **2017**, 33 (19), 4628–4637.
- (70) Dallin, B. C.; Van Lehn, R. C. Spatially Heterogeneous Water Properties at Disordered Surfaces Decrease the Hydrophobicity of Nonpolar Self-Assembled Monolayers. *J. Phys. Chem. Lett.* **2019**, *10*, 3991–3997.
- (71) Segawa, T.; Kateb, F.; Duma, L.; Bodenhausen, G.; Pelupessy, P. Exchange Rate Constants of Invisible Protons in Proteins Determined by NMR Spectroscopy. *ChemBioChem* **2008**, 9 (4), 537–542.
- (72) Tuchsen, E.; Woodward, C. Hydrogen Exchange of Primary Amide Protons in Basic Pancreatic Trypsin Inhibitor Evidence for Amino Group Rotation in Buried Asparagine Side Chains. *Biochemistry* **1987**, *26* (25), 8073–8078.
- (73) Wang, R. L. C.; Kreuzer, H. J.; Grunze, M. Molecular Conformation and Solvation of Oligo(Ethylene Glycol)-Terminated Self-Assembled Monolayers and Their Resistance to Protein Adsorption. J. Phys. Chem. B 1997, 101 (47), 9767–9773.
- (74) Hayashi, T.; Tanaka, Y.; Koide, Y.; Tanaka, M.; Hara, M. Mechanism Underlying Bioinertness of Self-Assembled Monolayers of Oligo(Ethyleneglycol)-Terminated Alkanethiols on Gold: Protein Adsorption, Platelet Adhesion, and Surface Forces. *Phys. Chem. Chem. Phys.* **2012**, *14* (29), 10196–10206.
- (75) Nagasawa, D.; Azuma, T.; Noguchi, H.; Uosaki, K.; Takai, M. Role of Interfacial Water in Protein Adsorption onto Polymer Brushes as Studied by SFG Spectroscopy and QCM. *J. Phys. Chem. C* **2015**, 119 (30), 17193–17201.